A&A 448, 489–498 (2006)
DOI: 10.1051/0004-6361:20053928

Astronomy & Astrophysics

Massive star formation in the central regions of spiral galaxies⋆

J. H. Knapen[1], L. M. Mazzuca[2], T. Böker[3], I. Shlosman[4], L. Colina[5], F. Combes[6], and D. J. Axon[1,7]

[1] Centre for Astrophysics Research, University of Hertfordshire, Hatfield, Herts AL10 9AB, UK
e-mail: j.knapen@star.herts.ac.uk
[2] NASA Goddard Space Flight Center, Code 441, Greenbelt, MD 20771, USA
[3] ESA/ESTEC, Keplerlaan 1, 2200 AG Noordwijk, The Netherlands
[4] Department of Physics and Astronomy, University of Kentucky, Lexington, KY 40506-0055, USA
[5] Instituto de Estructura de la Materia, CSIC, Serrano 119, 28006 Madrid, Spain
[6] Observatoire de Paris, 61 Av. de l'Observatoire, 75014 Paris, France
[7] Department of Physics, Rochester Institute of Technology, 84 Lomb Memorial Drive, Rochester, NY 14623, USA

Received 27 July 2005 / Accepted 27 October 2005

ABSTRACT

Context. The morphology of massive star formation in the central regions of galaxies is an important tracer of the dynamical processes that govern the evolution of disk, bulge, and nuclear activity.
Aims. We present optical imaging of the central regions of a sample of 73 spiral galaxies in the Hα line and in optical broad bands, and derive information on the morphology of massive star formation.
Methods. We obtained images with the William Herschel Telescope, mostly at a spatial resolution of below one second of arc. For most galaxies, no Hα imaging is available in the literature. We outline the observing and data reduction procedures, list basic properties, and present the *I*-band and continuum-subtracted Hα images. We classify the morphology of the nuclear and circumnuclear Hα emission and explore trends with host galaxy parameters.
Results. We confirm that late-type galaxies have a patchy circumnuclear appearance in Hα, and that nuclear rings occur primarily in spiral types Sa-Sbc. We identify a number of previously unknown nuclear rings, and confirm that nuclear rings are predominantly hosted by barred galaxies.
Conclusions. Other than in stimulating nuclear rings, bars do not influence the relative strength of the nuclear Hα peak, nor the circumnuclear Hα morphology. Even considering that our selection criteria led to an over-abundance of galaxies with close massive companions, we do not find *any* significant influence of the presence or absence of a close companion on the relative strength of the nuclear Hα peak, nor on the Hα morphology around the nucleus.

Key words. galaxies: spiral – galaxies: structure – galaxies: nuclei

1. Introduction

Enhanced nuclear activity in disk galaxies, in starburst or AGN form, appears to be an integral part of their evolution. Both forms of activity have been observed to co-exist (e.g., Heckman et al. 1997) and are a clear manifestation of the symbiotic evolution of galactic centres and their host galaxies. The observed tight correlation between the masses of the central black holes and the velocity dispersions in the surrounding bulges (e.g., review by Ferrarese & Ford 2005) provides the most direct evidence for this evolution and yields important clues on the dynamics, structure, and evolution of galaxies.

To initiate and to maintain the AGN or nuclear starburst activity, gas inflow must be stimulated from the disk to the central regions – a process which must be accompanied by a substantial loss of angular momentum in the gas. Theoretically, this leads to the suggestion that gravitational torques acting through galactic bars or galaxy interactions are involved. Due to the asymmetric nature of their mass distribution, they can facilitate the loss of angular momentum in inflowing material (e.g., Shlosman et al. 1990; Athanassoula 1994; Combes 2001). Observationally, statistical links between bars and interactions on the one hand and the occurrence of starburst and AGN activity on the other are clear in certain circumstances (e.g., extreme starbursts and interactions), barely significant in others (e.g., low-*L* AGN and bars; low-*L* starbursts and interactions), and absent in the case of low-*L* AGN and interactions (e.g., review by Knapen 2004).

Massive SF can be convincingly traced by the accompanying Hα emission and is very easily observed with standard telescopes and cameras (Kennicutt 1998). Hα is mainly produced in the H II regions surrounding massive B and O stars, although

⋆ Figure 1 is only available in electronic form at
http://www.edpsciences.org

shocks and non-stellar activity can also lead to Hα emission. In the images of the 73 galaxies analysed here, we study the morphology of the Hα emission in the circumnuclear, two kpc radius regions, as well as from the nucleus per se. The circumnuclear area as chosen is large enough to incorporate most nuclear rings. Such circumnuclear, low-L starbursts are found in around one fifth of spiral galaxies (Knapen 2005, hereafter K05), and characterise the dynamics of the host galaxy and its stellar bar (e.g., Buta & Combes 1996; K05).

We present our galaxy sample in Sect. 2, and describe the observations and data reduction procedures in Sect. 3. The nuclear and circumnuclear Hα morphology is analysed in Sects. 4 and 5, and relations to host galaxy properties, such as the presence of bars and nuclear activity, the morphological type, and the presence of companion galaxies, is discussed in Sect. 6. Section 7 lists our main conclusions. In a subsequent Paper II (Mazzuca et al., in preparation) we will further investigate the morphology and stellar ages in the 22 nuclear rings which we have identified in the course of this study.

2. Sample selection and parameters

For this study, we selected galaxies with some prior evidence for Hα structure in their central regions, either from the literature or from our own unpublished work. Since one of the aims of the current study is to identify nuclear rings, we have included a number of galaxies with known nuclear or inner rings, some of which have also been described in the works by Pogge (1989a,b), Buta & Crocker (1993), or K05. The observed sample is therefore not complete and any results must be interpreted with the appropriate care. For instance, the sample selection procedure will not allow a determination of the fraction of, say, nuclear rings in spiral galaxies.

The final sample, as observed by us with the William Herschel Telescope (WHT), consists of 73 galaxies spanning a range in many basic parameters, for which we obtained Hα, B and I imaging (see next Section for details). The galaxy sample is presented in Table 1, which also lists a number of important observational parameters as obtained from the literature. From the RC3 (de Vaucouleurs et al. 1991) we obtained the morphological type (Col. 2 in Table 1), the apparent major isophotal diameter measured at or reduced to surface brightness level $\mu_B = 25.0$ B-mag arcsec^{-2}, D_{25} (in arcmin, Col. 4), and the inclination and major axis position angle (in degrees, Cols. 5 and 6). From the NASA/IPAC extragalactic database (NED) we obtained a descriptor of the nuclear activity of the galaxy, for which we will distinguish between the four main categories Seyfert, LINER, starburst or HII, and none (Col. 2). The recession velocity (in km s^{-1}, Col. 7) was obtained from the RC3 for most galaxies, but from the NED for those where the RC3 does not list a value.

The distance D to a galaxy (in Mpc, Col. 8) was taken from the Nearby Galaxies Catalog (Tully 1988) whenever a value was given there; if not, we derived it from the recession velocity assuming a Hubble constant of $H_0 = 75$ km s^{-1} Mpc^{-1}. We used the distance to derive the image scale, in parsec per arcsec (Col. 10). The absolute blue magnitude (M_B, Col. 11) was taken from Tully (1988), or derived from the distance where a galaxy is not included in the Tully (1988) catalogue. As an indicator of bar strength, we list the gravitational bar torque parameter $Q_{\rm b}$ (Col. 12), as obtained from various papers (see caption to Table 1 for details; and Buta & Block 2001; and Block et al. 2004, for a description of $Q_{\rm b}$).

Finally, we list in Table 1 (Col. 16) whether a galaxy has a close companion or not. The criterion for classifying a sample galaxy as having such a companion is that it must have at least one neighbouring galaxy within a radius of five times the diameter of the galaxy under consideration, or $r_{\rm comp} < 5 \times D_{25}$, where D_{25} is listed in Col. 2 of Table 1. Any companion must also have a recession velocity within a range of ± 200 km s^{-1} of the sample galaxy, and be not more than three magnitudes fainter. These criteria have evolved from those used by Schmitt (2001), Laine et al. (2002) and K05, and ensure that companion galaxies are not only nearby, but also massive enough to have a gravitational impact on the sample galaxy. The search for qualifying neighbouring galaxies was performed using the "near name" search option in the NED.

We find that 26 of our 73 galaxies have a close companion (36%). This is a rather high number, no doubt influenced by the fact that we have been selecting galaxies with previous evidence for "interesting" structure in their central regions, and also by the fact that our sample spans a considerable range in distance. In comparison, only 48 (15%) out of the 327 galaxies which comprise the statistically complete sample of local galaxies in the HaGS (Hα Galaxy Survey, James et al. 2004) show a close companion under the same criteria as used here (Knapen & James, in preparation).

3. Observations and data reduction

All the imaging presented in this paper has been obtained using the Auxiliary Port (Aux Port) camera on the 4.2 m WHT, operated by the Isaac Newton Group in La Palma. The bulk of the imaging was obtained during a total of four observing nights granted by the UK time allocation panel (1999 September 16 and 17, and 2000 July 25 and 26), with additional imaging obtained in service mode during a number of nights in 1999 and 2000. We also used images of a few galaxies (e.g., NGC 4314 and NGC 4321) obtained by one of us (*JHK*) during earlier observing runs with the WHT. The images of NGC 4321 have been published before by Knapen et al. (1995a,b).

The Aux Port camera is a small optical camera without any re-imaging optics located at a dedicated folded cassegrain focus of the WHT. Its small pixel scale (0.11 arcsec/pixel) combined with a 1024×1024 pixel TEK CCD and round filters yields a circular field of view (FOV) of about 1.8 arcmin in diameter. We used Harris B and I filters, and one of the narrowband filters 6570/55, 6594/44, 6607/50, 6626/44 or 6656/44, depending on the systemic velocity of the galaxy, where the numbers denote $\lambda/\Delta\lambda$, or the central wavelength of transmission and the width of the transmission curve, both in Å. We used typical exposure times of 1, 3, and 10 min in I and B, and Hα, respectively. Atmospheric conditions were good in general, and the resulting spatial resolution as measured from the reduced images is around 0.8 arcsec in the Hα and I-band images, and around 1.0 arcsec in B.

Table 1. Global parameters of the galaxies in the observed sample, obtained from the RC3 unless otherwise indicated. Tabulated are the identification number of the sample galaxies (all are NGC numbers except IC 1438; Col. 1); the morphological type (Col. 2); nuclear activity class (from NED; Col. 3); D_{25}, the apparent major isophotal diameter measured at or reduced to surface brightness level $\mu_B = 25.0$ B-mag arcsec^{-2} (Col. 4); inclination i as derived from the ratio of the major to the minor isophotal diameter (Col. 5); position angle PA of the disk (Col. 6); mean heliocentric radial velocity v, in a few cases obtained from NED (Col. 7); distance D in Mpc (Col. 8); reference for D, where 1 is v from Col. 7 and assuming a Hubble constant of $H_0 = 75$ km s^{-1} Mpc^{-1}, 2 is the Nearby Galaxies Catalog (Tully 1988; Col. 9); image scale in parsec per arcsec, as derived from the distance (Col. 10); absolute blue magnitude, taken from Tully (1988) whenever possible, otherwise derived from m_B (from the RC3) and the distance (Col. 11); gravitational bar torque Q_b (Col. 12); reference for Q_b (Col. 13), where 3 is Laurikainen & Salo (2002), 4 is Block et al. (2001), 5 is Buta & Block (2001), 6 is Block et al. (2004), 7 is Laurikainen et al. (2004), 8 is Buta et al. (2005). An average is given when more than one measure is available in the literature, except where a value is available from Block et al. (2004) or Buta et al. (2005), which are given without taking earlier determinations into account; morphological classification of the nuclear (Col. 14; where "N" means no emission, "W" weak, "S" strong, and "P" position; see Sect. 4.1) and circumnuclear Hα emission (Col. 15; "D" means diffuse, "P" patchy, "N" none, "R" ring; see Sect. 4.2), and whether a galaxy is classed as having a close companion ("Y") or not ("N"; Col. 16; see Sect. 2).

NGC	Type	Activity (NED)	D_{25} (′)	i (°)	PA (°)	v (km s^{-1})	D (Mpc)	Ref. (D)	Scale (pc/″)	M_B	Q_b	Ref. (Q_b)	Morph. N	Morph. CN	Comp.
128	.L...P/		3.0	72	1	4241	56.6	1	274.1	–20.99			N	P	Y
157	.SXT4..		4.2	50	40	1668	20.9	2	101.3	–20.06	0.33	8	W	P	N
210	.SXS3..		5.0	49	160	1634	20.3	2	98.4	–20.06	0.05	8	N	P	Y
255	.SXT4..		3.0	34	15	1600	20.0	2	97.0	–19.26			N	P	N
278	.SXT3..		2.1	17		641	11.8	2	57.2	–19.62	0.05	8	N	R	N
470	.SAT3..	HII	2.8	52	155	2374	30.5	2	147.9	–20.05			N	P	Y
473	.SXR0*.		1.7	51	153	2133	29.8	2	144.5	–19.77			W	R	N
488	.SAR3..		5.2	42	15	2269	29.3	2	142.1	–21.36	0.03	8	S	N	N
613	.SBT4..	Sy	5.5	41	120	1475	17.5	2	84.8	–20.53	0.30	8	S	R	N
628	.SAS5..		10.5	24	25	656	9.7	2	47.0	–20.32	0.02	4	W	P	N
772	.SAS3..		7.2	54	130	2458	32.6	2	158.0	–21.80	0.1	3	S	P	Y
788	.SAS0*.	Sy2	1.9	41	75	4078	54.4	1	263.6	–20.68			S	N	N
864	.SXT5..		4.7	41	20	1560	20.0	2	97.0	–20.20	0.32	8	S	P	N
922	.SBS6P.		1.9	36		3092	41.2	1	199.9	–20.63			N	P	Y
925	.SXS7..	HII	10.5	56	102	553	9.4	2	45.6	–19.66			N	P	N
1042	.SXT6..		4.7	39	15	1373	16.7	2	81.0	–19.91	0.04	8	W	P	Y
1068	RSAT3..	Sy1 Sy2	7.1	32	70	1137	14.4	2	69.8	–21.39	0.16	3, 7	S	P	Y
1073	.SBT5..		4.9	24	15	1211	15.2	2	73.7	–19.44	0.56	8	N	P	N
1079	RSXT0P.		3.5	52	87	1447	16.9	2	81.9	–18.83			S	P	N
1084	.SAS5..		3.2	56	115	1406	17.1	2	82.9	–20.26	0.04	8	S	P	N
1087	.SXT5..		3.7	53	5	1519	19.0	2	92.1	–20.21	0.43	8	S	P	N
1140	.IB.9P*	HII Sy2	1.7	57	6	1509	18.2	2	88.2	–18.77			S	P	N
1232	.SXT5..		7.4	29	108	1682	20.0	2	97.0	–21.11	0.21	7	N	N	N
1241	.SBT3..	Sy2	2.8	53	145	4030	26.6	2	129.0	–19.83	0.18	8	S	P	Y
1300	.SBT4..		6.2	49	106	1568	18.8	2	91.1	–20.42	0.52	8	W	R	Y
1302	RSBR0..		3.9	17		1703	20.0	2	97.0	–20.11	0.06	8	S	N	N
1343	.SXS3*P		2.6	51	80	2215	29.5	1	143.2	–18.85			W	R	N
1398	PSBR2..	Sy	7.1	41	100	1407	16.1	2	78.1	–20.57	0.2	3, 7	S	N	N
1530	.SBT3..		4.6	58		2461	36.6	2	177.4	–21.32	0.71	6	N	R	N
1637	.SXT5..		4.0	36	15	717	8.9	2	43.1	–18.33	0.19	8	S	P	N
3982	.SXR3*.		2.3	29		1109	17.0	2	82.4	–18.65			S	P	N
4303	.SXT4..	HII Sy2	6.5	27		1569	15.2	2	73.7	–20.71	0.08	8	S	R	N
4314	.SBT1..	LINER	4.2	27		963	9.7	2	47.0	–18.65	0.44	8	S	R	Y
4321	.SXS4..	LINER HII	7.4	32	30	1586	16.8	2	81.4	–21.13	0.18	3, 4, 5, 7	S	R	Y
5248	.SXT4..	Sy2 HII	6.2	44	110	1153	22.7	2	110.1	–21.07	0.06	8	S	R	N
5383	PSBT3*P	Sbrst	3.2	32	85	2250	37.8	2	183.3	–20.96			N	P	N
5430	.SBS3..	HII Sbrst	2.2	58	0	2961	39.5	1	191.4	–20.11			N	P	N
5457	.SXT6..		28.8	21		241	5.4	2	26.2	–20.45	0.125	3, 5	N	P	Y
5701	RSBT0..	LINER	4.3	17		1506	26.1	2	126.5	–20.35	0.14	8	S	N	N
5728	.SXR1*.	Sy2	3.1	55	0	2788	42.2	2	204.6	–21.67			S	R	N
5730	.I..9*.		1.8	78	88	2533	33.8	1	163.7	–18.01			N	P	Y
5850	.SBR3..		4.3	29	140	2556	28.5	2	138.2	–20.69	0.31	8	S	P	Y
5905	.SBR3..	Sy1	4.0	49	135	3390	45.2	1	219.1	–20.69	0.43	5	N	R	Y

Table 1. continued.

NGC	Type	Activity (NED)	D_{25} (′)	i (°)	PA (°)	v (km s^{-1})	D (Mpc)	Ref. (D)	Scale (pc/″)	M_B	Q_b	Ref. (Q_b)	Morph. N	Morph. CN	Int.
5921	.SBR4..	LINER	4.9	36	130	1480	25.2	2	122.2	–20.67	0.26	8	S	P	N
5945	.SBT2..		2.1	21	105	5516	73.6	1	356.6	–20.63			S	R	Y
5953	.SA.1*P	LINER Sy2	1.6	34	169	1965	33.0	2	160.0	–19.59			S	R	Y
5970	.SBR5..	LINER HII	2.9	47	88	1963	31.6	2	153.2	–20.55			N	P	Y
5982	.E.3...		2.6	41	110	3017	40.2	1	195.0	–20.98			S	N	Y
6217	RSBT4..	Sy2	3.0	34		1362	23.9	2	115.9	–20.19	0.39	3	S	P	N
6384	.SXR4..	LINER	6.2	49	30	1663	26.6	2	129.0	–21.31	0.14	8	S	N	N
6412	.SAS5..		2.5	29		1324	23.5	2	113.9	–19.69			N	P	N
6503	.SAS6..	LINER HII	7.1	70	123	44	6.1	2	29.6	–18.64			W	R	N
6574	.SXT4*.	Sy	1.4	39	160	2282	35.0	2	169.7	–20.76			W	P	N
6814	.SXT4..	Sy1.5	3.0	21		1563	22.8	2	110.5	–20.41			S	P	N
6907	.SBS4..		3.3	36	46	3161	42.2	1	204.3	–21.22	0.07	8	S	P	N
6946	.SXT6..	HII	11.5	32		52	5.5	2	26.7	–20.78	0.04	4	S	P	N
6951	.SXT4..	LINER Sy2	3.9	34	170	1426	24.1	2	116.8	–20.73	0.39	6	S	R	N
7130	.S..1P.	LINER Sy2	1.5	24		4842	64.6	1	313.0	–21.13			S	P	N
7217	RSAR2..	LINER Sy	3.9	34	95	946	16.0	2	77.6	–20.38	0.03	8	S	R	N
IC 1438	PSXT1*.		2.4	32		2616	33.8	2	163.9	–20.08			W	R	Y
7331	.SAS3..	LINER	10.5	69	171	821	14.3	2	69.3	–21.10	0.12	3	S	P	Y
7469	PSXT1..	Sy1.2	1.5	44	125	4916	65.6	1	317.8	–21.08			S	R	Y
7479	.SBS5..	LINER Sy2	4.1	41	25	2378	32.4	2	157.1	–21.11	0.70	8	S	P	N
7550	.LA.-..	AGN	1.4	29		5072	67.6	1	327.9	–20.99			W	N	Y
7570	.SB.1..		1.5	54	30	4698	62.6	1	303.7	–20.09			N	R	N
7606	.SAS3..		5.4	67	145	2233	28.9	2	140.1	–21.28	0.09	3	S	D	N
7672	.S..3..	Sy2	1.2	41		4010	53.5	1	259.2	–18.94			S	P	Y
7716	.SXR3*.		2.1	34	35	2571	33.7	2	163.4	–19.84			S	R	N
7723	.SBR3..		3.5	47	35	1875	23.7	2	114.9	–20.29	0.32	8	S	P	N
7727	.SXS1P.		4.7	41	35	1814	23.3	2	113.0	–20.38	0.09	8	S	D	Y
7741	.SBS6..		4.4	47	170	755	12.3	2	59.6	–18.76	0.74	8	P	P	N
7742	.SAR3..	LINER HII	1.7	0		1653	22.2	2	107.6	–19.65			S	R	N
7769	RSAT3..	LINER HII	1.7	17		4214	56.2	1	272.4	–20.93			S	P	Y

The data reduction process followed basic procedures for bias subtraction and flat fielding using twilight sky flat fields. Image registration was done by measuring the positions of foreground stars where available, and the centre of the galaxy in all cases. For the subtraction of the continuum from the Hα images we used the *I*-band images. We determined the scaling factor by applying the procedure described by Böker et al. (1999) to all individual sets of Hα + *I* images. This method uses the fact that most pixels in any set of two registered images of a galaxy will show continuum emission, whereas only a minority show continuum plus line emission. When plotting all individual pixels, those tracing the continuum will scatter along a narrow, well-defined band, the slope of which denotes the scaling factor to be used for the continuum subtraction. Pixels containing Hα emission will end up above this band (assuming that Hα intensity is plotted as the ordinate). We refer the reader to the papers by Böker et al. (1999) and Knapen et al. (2004a) for a more detailed description. Knapen et al. (2004a) discuss the uncertainties introduced by using *I*-band imaging for continuum subtraction, and conclude that the resulting errors in the luminosities of HII regions are smaller than some 5%, and that the resulting Hα morphology is reliable.

The *I*-band and continuum-subtracted Hα images of all sample galaxies are shown in Fig. 1 (published electronically). The *B*-band images (not shown here) generally outline a morphology similar to that shown in Hα, though less pronounced in showing the star forming regions.

4. Hα morphology: methodology and limitations

4.1. Nuclear Hα emission

We have chosen to limit the classification of the nuclear Hα morphology to three categories: strong, weak, and none. This is mainly because of the uncertainties in the continuum subtraction using *I*-band images in the very centres of our galaxies, where differential dust extinction can play a more prominent role than in the disk (Knapen et al. 2004a). These classifications apply to the central point source – in practise the nuclear region of one seeing element in size. The exact position of the nucleus in a galaxy was determined from the *I*-band image. To qualify as a strong Hα source, a nuclear point source must be more luminous than any other Hα-emitting region in the galaxy. To qualify as weak, a nuclear Hα peak must be present but stronger peaks are found outside the nucleus. Obviously, our category "none" describes those cases where no believable Hα emission can be observed from the nucleus. In one case (that of NGC 7741) we could not pinpoint the

location of the nucleus (not even using the near-IR image from Knapen et al. 2003), and this galaxy is thus not included in the following discussion.

4.2. Circumnuclear Hα morphology

For the purpose of this paper, we consider the morphology of the Hα emission in the circumnuclear region as that arising from outside the nucleus and within a radius of 2.0 kpc from the nucleus of the galaxy. The range in distances to our sample galaxies, from 5 to 74 Mpc (Table 1), implies that this 2 kpc radius corresponds to a range of linear sizes in our images, varying roughly from 77 arcsec to 6 arcsec. The Hα morphology was classified by visual inspection of the images within the appropriate radial area independently by two of the authors of this paper.

We used a minimal number of different morphological classes, following the scheme introduced by K05. The main categories are, first, "none", where obviously no Hα emission is detected in the circumnuclear region (there will usually be emission from the nucleus). Second, "patchy", where individual and clearly delimited patches of Hα emission are detected, tracing individual H II regions, but not in an obvious ring pattern. The "patchy" class includes galaxies where the circumnuclear H II regions form a spiral pattern, but because such a pattern is hard to classify simply and unambiguously, we have not explicitly classified such cases as spiral. Third, "ring", which denotes Hα emission organised into a well-defined nuclear ring. In three galaxies, circumnuclear Hα is detected which is not confined to individual patches, and these three galaxies have been classified "diffuse". The classifications are given in Table 1.

Of the 22 nuclear ring galaxies reported here, to the extent of our knowledge three have not been reported as nuclear ring hosts in the literature: NGC 473, NGC 5953, and NGC 7716.

The classification scheme used here is rather coarse, but we believe that it offers a good compromise between the need for classification and the enormous variety encountered in the detailed Hα morphology from galaxy to galaxy. This variety is no doubt partly due to the nature of Hα emission – originating in regions of massive star formation whose ionised gas emission will show a strong time evolution.

We will not discuss the fractions of galaxies in our sample which show patchy, ring-shaped, or no Hα emission, because the selection criteria of our sample imply that any conclusions from such a discussion would have no wider significance. This is in contrast to the study of K05, where the selection of a statistically meaningful sample leads, for instance, to the result that one of every five spiral galaxies has a nuclear ring. What the current sample can be used for, except of course for selecting sub-samples of specific interest, or for referring to individual objects, is an analysis of how a certain circumnuclear Hα morphology is distributed with respect to host galaxy parameters such as morphological class or presence of a bar, provided that reference is made to the distribution of such parameters across the whole sample under consideration (next section).

Table 2. Median values of the host galaxies' diameter (in arcmin, from the RC3; Col. 3), distance (in Mpc, from Tully 1988; Col. 4), absolute magnitude (calculated using m_B from the RC3 and the distance; Col. 5), and the gravitational bar strength Q_b (Col. 6), for the overall sample and the different classes of nuclear and circumnuclear emission (Col. 1; the number of galaxies in each category is shown in Col. 2). The last two columns show the fractions of the different nuclear and circumnuclear Hα emission morphologies among those galaxies which have close companions (Col. 6) and those which do not (Col. 7), following the criteria set out in Sect. 2. Uncertainties are 1σ as determined from Poisson statistics.

Emission	N	D	d	M_B	Q_b	Companions?	
		(′)	(Mpc)	(mag)		Y (%)	N (%)
Overall sample							
	73	3.7	23.9	–20.4	0.18	36 ± 6%	64 ± 6%
Nuclear emission							
Strong	44	3.9	23.8	–20.6	0.16	32 ± 7%	68 ± 7%
Weak	10	3.4	24.5	–20.1	0.19	40 ± 15%	60 ± 15%
None	18	3.0	31.0	–20.1	0.21	44 ± 12%	56 ± 12%
Circumnuclear emission							
Patchy	39	3.5	22.8	–20.2	0.19	36 ± 8%	64 ± 8%
None	9	4.3	26.6	–21.0	0.14	22 ± 14%	78 ± 14%
Ring	22	3.5	26.5	–20.4	0.30	36 ± 10%	64 ± 10%
Diffuse	3	4.7	28.9	–21.0	0.09	67 ± 27%	33 ± 27%

5. Hα morphology and host galaxy parameters

5.1. Overall results

The results on the overall distribution of the different Hα morphology classes are summarised in Table 2. Strong nuclear emission is found in 44 of our 73 sample galaxies, while 10 are classified as having weak nuclear Hα emission, and 18 as having no Hα emission at all. The circumnuclear Hα emission is patchy in more than half of our galaxies (39 out of 73), and in the form of a nuclear ring in 22. A further 9 galaxies show no circumnuclear Hα emission at all, and 3 have diffuse emission.

Table 2 also lists the median values of a number of key host galaxy parameters for the overall sample and for the different classes of nuclear and circumnuclear Hα emission. We have listed diameter, distance, absolute blue magnitude, and the bar's gravitational torque parameter Q_b, or bar strength, for those galaxies where this value is given in the literature. The only trend worth noting for the nuclear Hα emission is that those galaxies without Hα emission from the nucleus are, in the median, further away than those with emission, which is easily understood as related to sensitivity and detection. Those galaxies with strong Hα peaks in the nucleus are slightly brighter than others, but this may be a morphological type effect (see next section) and we will not discuss it in more detail.

As for the circumnuclear Hα emission, Table 2 shows how the 12 galaxies without, or with diffuse, Hα emission are both larger in diameter and fainter than the others. Those with patchy Hα emission are, in the median, at smaller distances from us. Using Q_b as an indicator, the galaxies with nuclear rings appear to have slightly stronger bars in the median, but

Table 3. Morphological and bar type distribution of the various types of circumnuclear Hα emission. For the whole sample and for the nuclear and circumnuclear emission, Col. 2 gives the total number of galaxies in each category (as described in Col. 1), with the number of galaxies of each morphological type (from the RC3) in Cols. 3−13, and bar type (from the RC3) in Cols. 14−17. In these four columns, the numbers in brackets are the percentages of the total. Note ⋆: see Sect. 5.5.

Emission	N	Morphological type T											Spiral type			
		0	1	2	3	4	5	6	7	8	9	–	SA	SX	SB	–
		S0	Sa	Sab	Sb	Sbc	Sc	Scd	Sd	Sdm	Sm	–	N (%)			
Total sample																
	73	5	8	3	22	14	10	6	1	0	2	2	16 (22)	28 (38)	24 (33)	5 (7)
Nuclear emission																
Strong	44	4	6	3	13	10	5	1	0	0	1	1	11 (25)	16 (36)	14 (32)	3 (7)
Weak	10	1	1	0	1	3	1	2	0	0	0	1	3 (30)	6 (60)	1 (10)	0 (0)
None	18	0	1	0	7	1	4	2	1	0	1	1	2 (11)	6 (33)	8 (44)	2 (11)
Position	1							1								
Circumnuclear emission																
Patchy	39	1	1	0	13	7	9	5	1	0	2	0	8 (21)	14 (36)	14 (36)	3 (8)
None	9	3	0	1	1	1	1	0	0	0	0	2	3 (33)	2 (22)	3 (33)	1 (11)
Ring	22	1	6	2	6	6	0	1	0	0	0	0	4⋆ (18)	11 (50)	7 (32)	0 (0)
Diffuse	3	0	1	0	1	0	0	0	0	0	0	1	1 (33)	1 (33)	0 (0)	1 (33)

a Kolmogorov-Smirnov (KS) test[1] shows that this difference is not statistically significant.

We also list the percentages of galaxies in the different categories which have nearby companions. Taking into account the numbers of galaxies in the different categories, the presence or absence of a close companion influences *neither* the nuclear, *nor* the circumnuclear Hα morphology. We will discuss this result, and its implications, in more detail in Sect. 5.3.

5.2. Morphological type of the host galaxy

5.2.1. T-type

Table 3 lists the distribution of the various classes of nuclear and circumnuclear morphology with spiral T-type, as obtained from the morphological classifications listed in the RC3 (the translation of T-type as used in the RC3 and more widely used descriptors of the type Sa, Sb, etc., is given in the header to Table 3). These results are shown as histograms in Figs. 2 and 3 for the circumnuclear and nuclear Hα morphology, respectively. The results confirm those presented by K05. The overall distribution of T-type for the sample shows a peak near types Sb and Sbc ($T = 3$ and 4, see Table 3), a broad distribution ranging from S0 to Sm, and a lack of galaxies of type Sdm. For 2 galaxies, no T-type is given in the RC3. We reiterate that no attempts were made at the sample selection stage to achieve a specific type distribution.

Galaxies with patchy *circumnuclear* Hα morphology tend to be of later types, and in fact there are only two galaxies of the 19 of type later than Sbc which are *not* classified as patchy (an Sc with no circumnuclear Hα, and an Scd with a ring). Ring-like morphology is preferentially found in earlier types, peaking at Sb and Sbc types. Galaxies with no circumnuclear Hα emission are also preferentially of early type, confirming the findings of K05.

Not much can be deduced from the distribution of *nuclear* Hα morphology with morphological type of the host galaxy (Fig. 3) because of the relatively low numbers of galaxies with weak, or no, nuclear Hα emission, but the T-type of the host does not seem to correlate with the presence of relative strength of the nuclear Hα emission.

5.2.2. Bars

The distribution of Hα morphology has been tabulated (Table 3) for the various bar classifiers used in the RC3: SA, SX (often quoted as SAB), and SB. Five galaxies have merely been classified as "S" in the RC3 and are not considered here. The distribution between SA, SX, and SB classes seen across the whole sample is closely mirrored in the sub-samples of different nuclear and circumnuclear Hα morphology. The numbers in the Table might appear to indicate a slight excess of SX galaxies among those with weak nuclear Hα, and a slight lack of SA galaxies among those with no nuclear emission. Poisson statistics show that in either case the significance of this difference is at most 1σ. Considering the same number from the perspective of non-barred vs. barred galaxies, we see that 69% ± 12% of the non-barred (SA) vs. 58% ± 7% of the barred (SX+SB) galaxies has "strong" nuclear Hα emission, 19% ± 10% vs. 13% ± 5% "weak", and 13% ± 8% vs. 27% ± 6% "none". Again, none of the differences are significant.

[1] The Kolmogorov-Smirnov test is a statistical test that describes the likelihood that two data sets have been drawn from the same parent distribution: a probability $P < 0.05$ is usually interpreted as describing two statistically distinct populations.

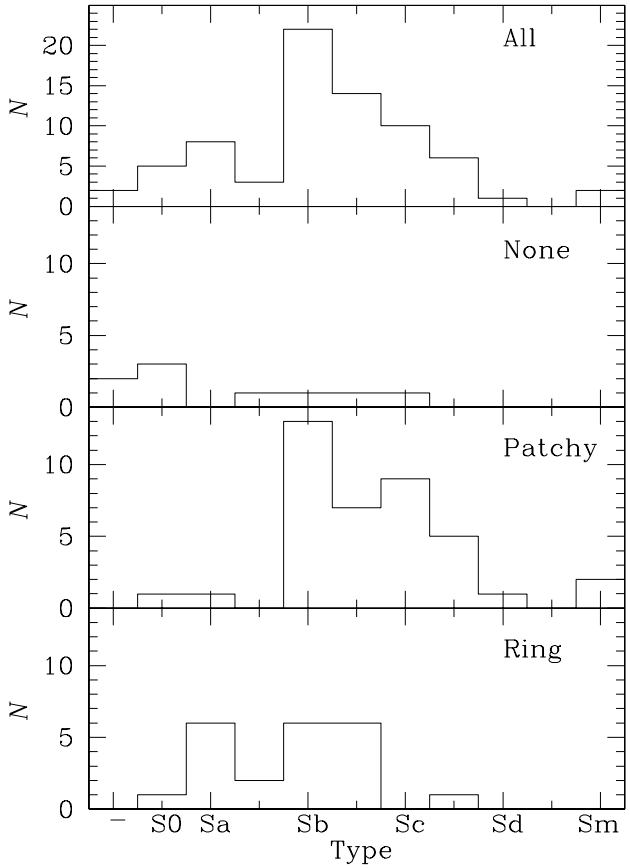

Fig. 2. Set of histograms showing the distribution of circumnuclear Hα emission morphology with host galaxy type, the latter obtained from the RC3.

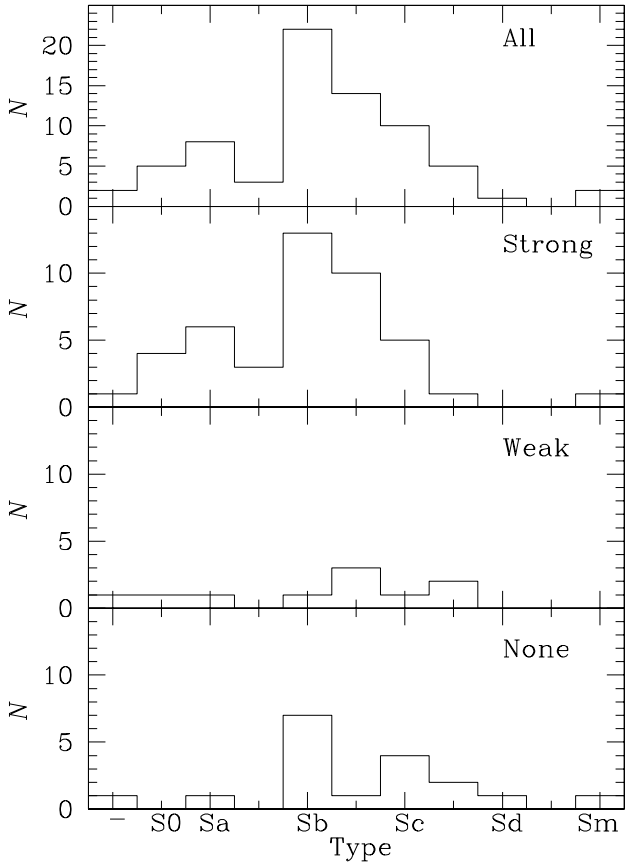

Fig. 3. As Fig. 2, now for the distribution of nuclear Hα emission morphology.

The bar distribution in the galaxies in the different classes of circumnuclear emission mirror those in the overall sample closely (the apparent deviations in the case of the three SA and two SX "none" galaxies are a 1σ effect). Table 3 shows explicitly how the percentages of barred and non-barred galaxies are rather stable for the different classes of morphology. Calculating the percentage of the different morphology classes for barred and non-barred galaxies, we see the same effect, for instance, 50%±13% of non-barred (SA) galaxies have a patchy circumnuclear Hα morphology, versus 54% ± 7% of barred galaxies (SX+SB). These numbers are 19%±10% vs. 10%±4% for "none"; and 25% ± 11% vs. 35% ± 7% for "ring" (but see below).

The galaxies hosting circumnuclear rings in Hα only show a rather moderate preference for SX and SB hosts, which at first sight may appear to be at odds with the findings of K05, who confirmed the standard picture that bars are almost exclusively responsible for the existence of nuclear rings. In fact, K05 pointed out that of the 12 nuclear ring hosts considered, only two have been originally classified as non-barred SA, but that each of those two has clear evidence from near-IR imaging for the existence of a bar. We will discuss the four SA-type nuclear ring host galaxies in the current sample in more detail in Sect. 5.5.

5.3. Close companions

In analysing the relations between our sample galaxies and whether or not they have nearby, relatively massive (defined in Sect. 2 as not more than 3 mag fainter than the sample galaxy) companions, we consider two related sets of numbers: those describing how many galaxies in each of our nuclear and circumnuclear Hα morphology categories has a close companion, and those describing the properties of the subsets of sample galaxies that either have, or do not have, a close companion. The result on the former, shown in Table 2 and already mentioned in Sect. 5.1, is that we find no significant differences in the numbers of galaxies that have close companions among our different categories of nuclear and circumnuclear Hα morphology. This is surprising, because one might have expected close companions and/or interactions to lead to enhanced massive star formation in, and thus Hα emission from, the nucleus, or nuclear rings (Knapen et al. 1995a; Buta & Combes 1996; Heller & Shlosman 1996; Knapen et al. 2004b). In fact, the only hint at such a general effect is the slightly lower fraction of galaxies with close companions among those with no circumnuclear emission, but with two out of nine galaxies causing the lower number in Table 2 we cannot call this deviation significant. We must conclude that *neither* the nuclear, *nor* the circumnuclear massive star formation morphology is at all affected by the presence of close companions.

Table 4. Median values of overall parameters of the interacting (see Sect. 2 for criteria) and non-interacting sample galaxies (sample sizes in Col. 2), as well as the numbers and percentages (latter in parentheses) of those galaxies in the different circumnuclear (Cols. 8−11) and nuclear (Cols. 12−14) Hα morphology classes. Parameters are diameter (in arcmin, from the RC3; Col. 3), distance (in Mpc, from Tully 1988; Col. 4), absolute magnitude (calculated using m_B from the RC3 and the distance; Col. 5), morphological type (from the RC3; Col. 6), and the gravitational bar strength Q_b (Col. 7).

	N	D	d	M_B	Type	Q_b	Circumnuclear Hα morph. (N(%))				Nuclear Hα morph. (N(%))		
		(′)	(Mpc)	(mag)			Patchy	None	Ring	Diff.	Strong	Weak	None
Close companion	26	2.9	32.1	−20.6	4.0	0.16	14 (54)	2 (8)	8 (31)	2 (8)	14 (54)	4 (15)	8 (31)
No close companion	47	3.9	22.7	−20.3	3.0	0.20	25 (53)	7 (15)	14 (30)	1 (2)	30 (64)	6 (13)	10 (21)

The results on the second test are summarised in Table 4, which compares the properties of those galaxies that have a close companion with those that do not. Columns 3 and 4 show that within our sample the galaxies with close companions are further away, and smaller in angular diameter, than those without close companions. This is related to the fact that the median absolute magnitude of the galaxies with close companions is brighter than that of the isolated galaxies, in the median by 0.3 mag in M_B. It is plausible that the combination of these differences implies that galaxies with close companions are brighter, and therefore more likely to be included in our sample at higher distances. Galaxies with a close companion are, in the median, also of later morphological T-type than those without a close companion. We performed KS tests on these data sets, and found that whereas the difference in distance between the two sub-samples is significant ($P = 0.029$), none of the other differences are (D, M_B, T).

Yet even though our "closely accompanied" galaxies are brighter, possibly because of enhanced star formation triggered by the interaction, the effects on the morphology of the current massive star formation in the nucleus and in the 2 kpc radius circumnuclear region are negligible. Table 4 confirms this by showing the same data as tabulated before in Table 2, but now analysed as percentages of the different Hα morphology classes occurring in the sample galaxies with, and without, a close companions. The percentages are remarkably similar, confirming our overall conclusion that the presence of a close companion has no influence on the morphology of massive star formation in and around the centre.

5.4. Starburst and AGN activity

We have scanned the NED for nuclear activity classifications of our sample galaxies. As explained in K05, the information from NED may not be as reliable as a uniformly conducted spectroscopic survey, although K05 showed that this did not significantly alter their results. In addition, our sample includes galaxies at larger distances than those in K05. More galaxies may thus not have been checked for nuclear activity in detail, and will hence, by default, have no nuclear activity classifier in the NED. The results are tabulated in Table 5, which shows that of our 73 sample galaxies, 31 have been classified as AGN of some sort (we include Seyfert, LINER, and "AGN" types in this category), with another 5 galaxies classed as starburst using various nomenclature, including "H II".

Table 5. Nuclear and circumnuclear Hα emission for different categories of nuclear activity, basically AGN (including LINER-type activity) and starburst. Column 2: total sample. Column 3: AGN, which includes all galaxies classified in NED as either Seyfert or LINER. Column 4: H II/SB, all galaxies classified by NED as starburst or H II (excluding those whose classification also includes a LINER or Seyfert which have been classed AGN). Column 5: all galaxies not classified as Seyfert or Liner. Column 6: as Col. 5, but now also excluding the galaxies of Col. 4.

	Total	AGN	H II/SB	non-AGN	non-AGN non-SB
Nuclear emission					
Sample size	72	31	5	41	36
Strong	44	26	1	18	17
Weak	10	3	–	7	7
None	18	2	4	16	12
Circumnuclear emission					
Sample size	73	31	5	42	37
Patchy	39	13	5	26	21
None	9	5	–	4	4
Ring	22	13	–	9	9
Diffuse	3	–	–	3	3

The results, then, show two interesting features which are worth discussing here. The first is the significantly higher fraction of AGN which show strong nuclear Hα emission. Only a handful of galaxies, in fact, show weak or no nuclear Hα emission. Any AGN should have Hα emission, but the absence in the few cases where we report it can be explained as a differential extinction effect. We use the significantly redder I-band for the subtraction of the continuum from the relatively bluer Hα line, which in a dust-extincted environment will lead to surplus subtraction. This will lead to artificially reduced Hα central peaks. Galaxies classified as starbursts (or "H II") but with "none" nuclear Hα emission may well suffer from the same effects. Another possibility is that the classification as AGN or starburst as given on the NED is in fact erroneous, but checking that is outside the scope of this paper.

The second interesting feature from Table 5 is the enhanced fraction of AGN among the nuclear ring host galaxies. Of the AGN, 42% have a ring, against 30% of the complete sample. Conversely, 59% of the ring galaxies have an AGN, versus 42% of the complete sample. K05 found a similar effect, but much

more marked; there, almost all nuclear rings were accompanied by AGN or starburst activity.

The ring-AGN connection occurs partly because both rings and AGN are most common among the early-type galaxies. Of our sample, 52 galaxies (71%) have $T \leq 4$ (Sbc), but 21 out of our 22 rings (95%) and 26 out of our 31 AGN (84%) are hosted by galaxies of such early types. This means that half of all $T \leq 4$ galaxies are AGN, and statistically 10.5 ring hosts will also host AGN. We concur with K05 in finding a higher number than this statistically expected one. As discussed in more detail by K05, the connection between rings and AGN is most likely to be through the availability and recent inflow of gas, which fuels both the massive star formation in the ring and nuclear activity. In this interpretation, the nuclear rings are merely a by-product of the gas inflow from the disk toward the very central region (Shlosman 2005). A fraction of the inflowing gas moves further inward, and is ultimately responsible for the AGN activity.

5.5. Nuclear rings and their dynamical origin

We identify 22 nuclear rings, three of which have not been reported in the literature so far (those in NGC 473, NGC 5953, and NGC 7716). These are star-forming nuclear rings, classified as such purely on the basis of our Hα imaging. There may be a small number of additional rings which are, for instance, too small, or too dusty to be picked up by our imaging (the latter category might well include NGC 1241, for which Böker et al. 1999, find a small nuclear ring in Paα which is absent from our Hα image). Of the 22 nuclear rings, Table 1 shows that four occur in galaxies classed as unbarred (NGC 5953, NGC 6503, NGC 7217, and NGC 7742). In addition, NGC 278, although classified as SX in the RC3, does not in fact have a bar. Knapen et al. (2004b) made a detailed study of this galaxy, and found from an analysis of near-IR and optical ground-based images, as well as of *Hubble Space Telescope* (*HST*) imaging, that there is no evidence at all for the presence of a bar. Radio 21 cm interferometry, however, showed that the outskirts of the galaxy have a severely irregular and disturbed morphology and kinematics in H I, indicative of at least a minor merger event in the recent history of the galaxy. Knapen et al. (2004b) postulate that this minor merger lies at the origin of the massive star forming in the nuclear ring, rather than a bar as is more conventional for nuclear ring hosts. Considering that the favoured formation scenario of a nuclear ring is one where the ring forms in the vicinity of inner Lindblad resonances set up by a non-axisymmetry in the gravitational potential, due to, e.g., a bar or an interaction (see, e.g., Athanassoula 1992; Knapen et al. 1995b; Buta & Combes 1996; Heller & Shlosman 1996; Knapen et al. 2004b), it is instructive to scrutinise the four cases identified here of nuclear rings in supposedly non-barred galaxies.

– NGC 5953 (classed as SA but interacting): this galaxy forms part of a small interacting group of galaxies with NGC 5954 (visible in Fig. 1) and UGC 9902. Hernández-Toledo et al. (2003) report the presence of a small (~60 pc) "bar-like central structure". As in the case of NGC 278, it is plausible that this interaction has led to the formation of the nuclear ring, and the disturbed and complex H I morphology and kinematics observed by Chengalur et al. (1994) lends support to this suggestion.
– NGC 6503 (classed as SA but inclined): this galaxy is rather inclined ($i = 70°$) and it is thus very unlikely that any bar can be detected from optical or near-IR imaging – we postulate from statistical grounds only that this ring galaxy is most likely to be in fact barred. The H I velocity field is regular (Shostak et al. 1981; van Moorsel & Wells 1985), but Bottema & Gerritsen (1997) find evidence for a separate kinematically distinct nuclear component. We find no close companion.
– NGC 7217 (classed as SA): this is a well-studied galaxy which in fact has three rings (e.g., Combes et al. 2004, and references therein). There is no evidence for a bar, but Merrifield & Kuijken (1994) reported the presence of the distinct counter-rotating disk population. Although this is evidence for a past merger history, its current gravitational effects are most probably limited. The velocity field as seen from H I mapping is regular (Verdes-Montenegro et al. 1995). Buta et al. (1995) and Combes et al. (2004) show that there is an oval distortion in this galaxy, which can explain the occurrence of its three rings (nuclear, inner, outer). This may well be an indicator of a historical, but now destroyed, bar.
– NGC 7742 (classed as SA): this is another well-known ring galaxy, without any evidence for a bar or other asymmetry (Rix & Zaritsky 1995; Kornreich et al. 1998). No H I velocity field is available from the literature. De Zeeuw et al. (2002) describe, on the basis of SAURON integral field spectroscopy, that the gaseous ring counter-rotates with respect to the central stellar component.

We thus summarise that of the four nuclear ring host galaxies classified as SA in the RC3, one is interacting, and one is too inclined to allow us to see any bar it may have. The remaining two galaxies (NGC 7217 and NGC 7742) do not have a bar. NGC 7217 has an oval distortion, which is able to maintain the nuclear ring, as shown by simulations (Combes et al. 2004). It is possible that the nuclear ring was formed during a recent bar episode, of which the oval distortion is the remnant. This scenario is supported by the presence of three rings in this galaxy, at the right resonant locations. NGC 7742 has not been studied in nearly as much detail, has no evidence for an oval, but does have counter-rotating gas and stars in the nuclear region.

NGC 278, although classified as SX in the RC3, does not have a bar, but does show clear evidence for a recent minor merger (Knapen et al. 2004b). We can thus conclude that none of the galaxies reported here challenges the standard scenario of nuclear ring formation to a significant degree. In this scenario, gas and ensuing massive SF accumulate near one or more inner Lindblad resonances, induced by an asymmetry in the gravitational potential of the host galaxy, in turn due to a bar or an interaction. Galaxies like NGC 278, NGC 7217, and NGC 7742 which appear at first sight bar-less and isolated, remain excellent test cases which warrant detailed studies.

In Paper II, we will present a detailed discussion of the properties of the 22 nuclear rings, and of how these properties relate to those of their host galaxies and of their host bars, where those exist. We will also discuss the identification and age determination of the individual H II region complexes or stellar clumps within the rings, and compare the observed age distribution around the rings to dynamical models of ring formation.

6. Conclusions

We obtained a set of images in the *B* and *I* broad bands and in Hα of a sample of 73 spiral galaxies. The data, obtained with the WHT and mostly at a spatial resolution of below an arcsec, are presented here, along with a classification of the morphology of the nuclear and circumnuclear Hα emission. Most galaxies have relatively strongly peaked nuclear Hα emission, and patchy emission from the 2 kpc radius circumnuclear region, the latter indicative of the presence of individual H II regions. We explore trends with host galaxy parameters, and confirm that late-type galaxies have a patchy circumnuclear appearance in Hα, and that nuclear rings occur primarily in spiral types Sa-Sbc. We identify a number of previously unknown nuclear rings. Although we report a number of cases where a nuclear ring is hosted by an unbarred galaxy, we confirm that nuclear rings are predominantly hosted by barred galaxies. Bars thus stimulate nuclear rings, but do not influence the relative strength of the nuclear Hα peak, nor other aspects of the circumnuclear Hα morphology. Even though our selection criteria led to an over-abundance of galaxies with close massive companions, the presence or absence of a close companion does not have *any* significant influence on the relative strength of the nuclear Hα peak, nor on the Hα morphology around the nucleus. A more detailed description of the stellar populations and dynamical origin of the nuclear rings described here will follow in Paper II. The images described here will be made available to the community.

Acknowledgements. J.H.K. acknowledges support from the Leverhulme Trust in the form of a Leverhulme Research Fellowship. We thank Dr. Koji Murakawa for assistance during the 1999 observing run. L.C. thanks the University of Hertfordshire for financial assistance. This research has been partially supported by NASA/LTSA 5-13063, NASA/ATP NAG5-10823, HST/AR-10284 and by NSF/AST 02-06251. The WHT is operated on the island of La Palma by the Isaac Newton Group in the Spanish Observatorio del Roque de los Muchachos of the Instituto de Astrofísica de Canarias. This research has made use of the NASA/IPAC Extragalactic Database (NED) which is operated by the Jet Propulsion Laboratory, California Institute of Technology, under contract with the National Aeronautics and Space Administration.

References

Athanassoula, E. 1992, MNRAS, 259, 345
Athanassoula, E. 1994, in Mass-Transfer Induced Activity in Galaxies, ed. I. Shlosman (Cambridge: Cambridge University Press), 143
Block, D. L., Puerari, I., Knapen, J. H., et al. 2001, A&A, 375, 761
Block, D. L., Buta, R., Knapen, J. H., et al. 2004, AJ, 128, 183
Böker, T., Calzetti, D., Sparks, W., et al. 1999, ApJS, 124, 95
Bottema, R., & Gerritsen, J. P. E. 1997, MNRAS, 290, 585
Buta, R., & Crocker, D. A. 1993, AJ, 105, 1344
Buta, R., & Combes, F. 1996, Fund. Cosmic Phys., 17, 95
Buta, R., & Block, D. L. 2001, ApJ, 550, 243
Buta, R., van Driel, W., Braine, J., et al. 1995, ApJ, 450, 593
Buta, R., Vasylyev, S., Salo, H., & Laurikainen, E. 2005, AJ, 130, 506
Chengalur, J. N., Salpeter, E. E., & Terzian, Y. 1994, AJ, 107, 1984
Combes, F. 2001, in Advanced Lectures on the Starburst-AGN, ed. I. Aretxaga, D. Kunth, & R. Mújica (Singapore: World Scientific), 223
Combes, F., García-Burillo, S., Boone, F., et al. 2004, A&A, 414, 857
de Vaucouleurs, G., de Vaucouleurs, A., Corwin, J. R., et al. 1991, Third reference catalogue of Bright galaxies (New York: Springer-Verlag) (RC3)
de Zeeuw, P. T., Bureau, M., Emsellem, E., et al. 2002, MNRAS, 329, 513
Ferrarese, L., & Ford, H. 2005, Space Sci. Rev., 116, 523
Heckman, T. M., Gonzalez-Delgado, R., Leitherer, C., et al. 1997, ApJ, 482, 114
Heller, C. H., & Shlosman, I. 1996, ApJ, 471, 143
Hernández-Toledo, H. M., Fuentes-Carrera, I., Rosado, M., et al. 2003, A&A, 412, 669
James, P. A., et al. 2004, A&A, 414, 23
Kennicutt, R. C. 1998, ARA&A, 36, 189
Knapen, J. H. 2004, Astrophys. Sp. Sc. Library, 319, 189
Knapen, J. H. 2005, A&A, 429, 141 (K05)
Knapen, J. H., Beckman, J. E., Shlosman, I., et al. 1995a, ApJ, 443, L73
Knapen, J. H., Beckman, J. E., Heller, C. H., Shlosman, I., & de Jong, R. S. 1995b, ApJ, 454, 623
Knapen, J. H., de Jong, R. S., Stedman, S., & Bramich, D. M. 2003, MNRAS, 344, 527 (Erratum 2004, MNRAS, 346, 333)
Knapen, J. H., Stedman, S., Bramich, D. M., Folkes, S. L., & Bradley, T. R. 2004a, A&A, 426, 1135
Knapen, J. H., Whyte, L. F., de Blok, W. J. G., & van der Hulst, J. M. 2004b, A&A, 423, 481
Kornreich, D. A., Haynes, M. P., & Lovelace, R. V. E. 1998, AJ, 116, 2154
Laine, S., Shlosman, I., Knapen, J. H., & Peletier, R. F. 2002, ApJ, 567, 97
Laurikainen, E., & Salo, H. 2002, MNRAS, 337, 1118
Laurikainen, E., Salo, H., Buta, R., & Vasylyev, S. 2004, MNRAS, 355, 1251
Merrifield, M. R., & Kuijken, K. 1994, ApJ, 432, 575
Pogge, R. W. 1989a, ApJ, 345, 730
Pogge, R. W. 1989b, ApJS, 71, 433
Rix, H., & Zaritsky, D. 1995, ApJ, 447, 82
Schmitt, H. R. 2001, AJ, 122, 2243
Shlosman, I., Begelman, M. C., & Frank, J. 1990, Nature, 345, 679
Shlosman, I. 2005, in The Evolution of Starbursts, ed. S. Hüttemeister, & E. Manthey (Melville: AIP), 223
Shostak, G. S., Willis, A. G., & Crane, P. C. 1981, A&A, 96, 393
Tully, R. B. 1988 (Cambridge and New York: Cambridge University Press)
van Moorsel, G. A., & Wells, D. C. 1985, AJ, 90, 1038
Verdes-Montenegro, L., Bosma, A., & Athanassoula, E. 1995, A&A, 300, 65

Online Material

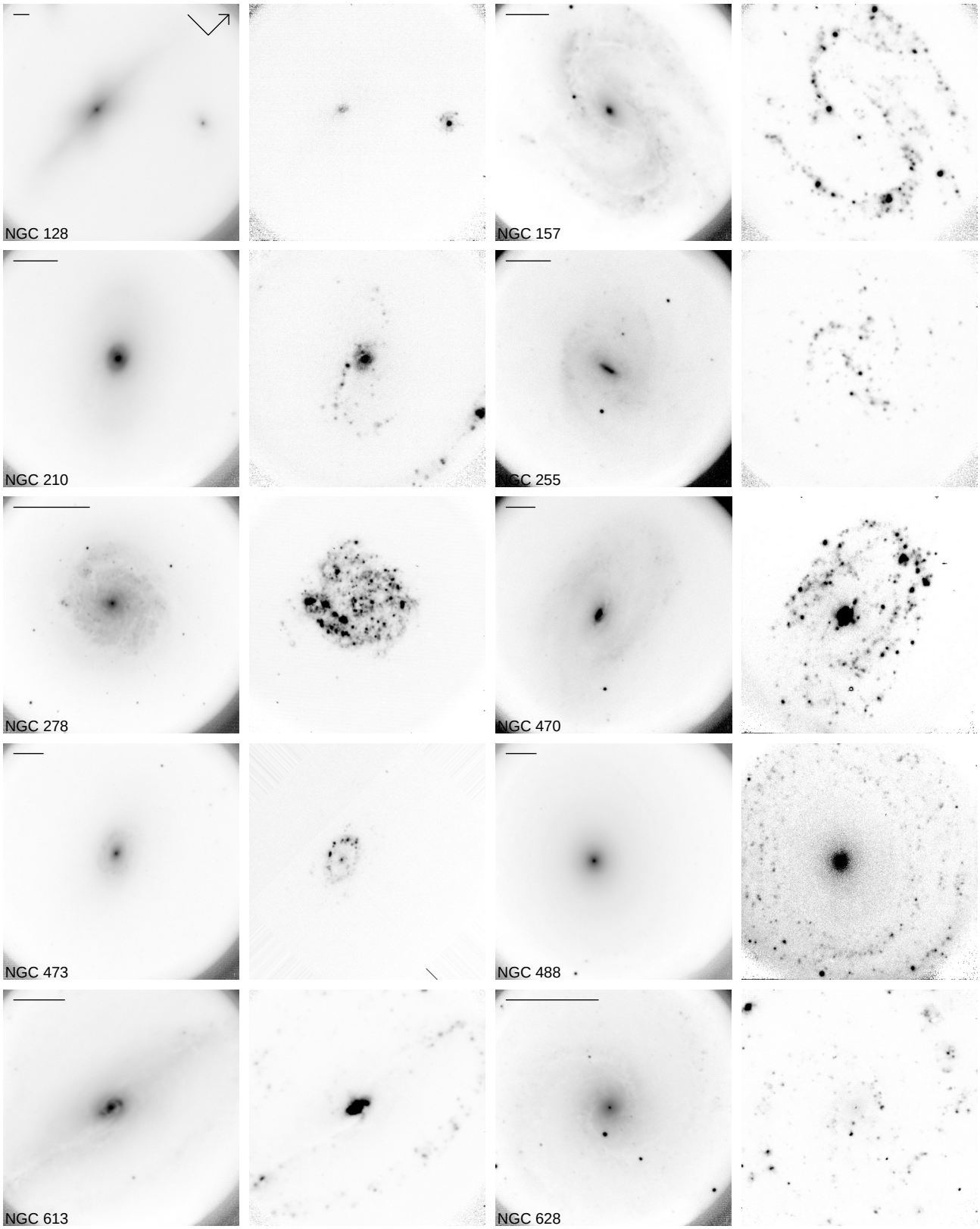

Fig. 1. Grey-scale representation of the *I*-band and continuum-subtracted Hα images of all sample galaxies, with the former shown on the left in each pair. The orientation is North up and East to the left, except for those cases where East and North are indicated in the upper right corner of the *I*-band image, and where the arrow points North. The scale is indicated for each galaxy by the length of the black line in the top left corner of the *I*-band image, which corresponds to 2 kpc.

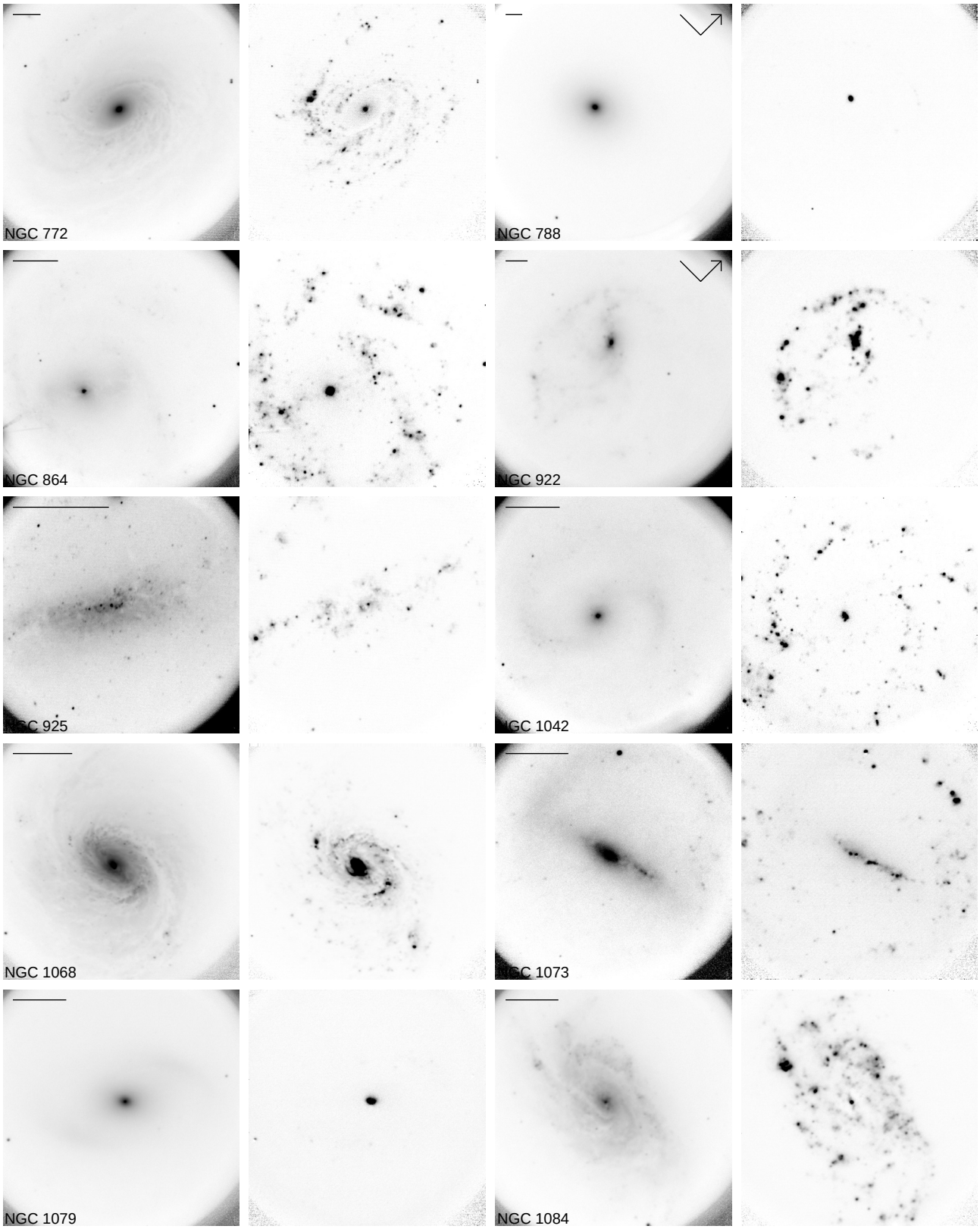

Fig. 1. continued.

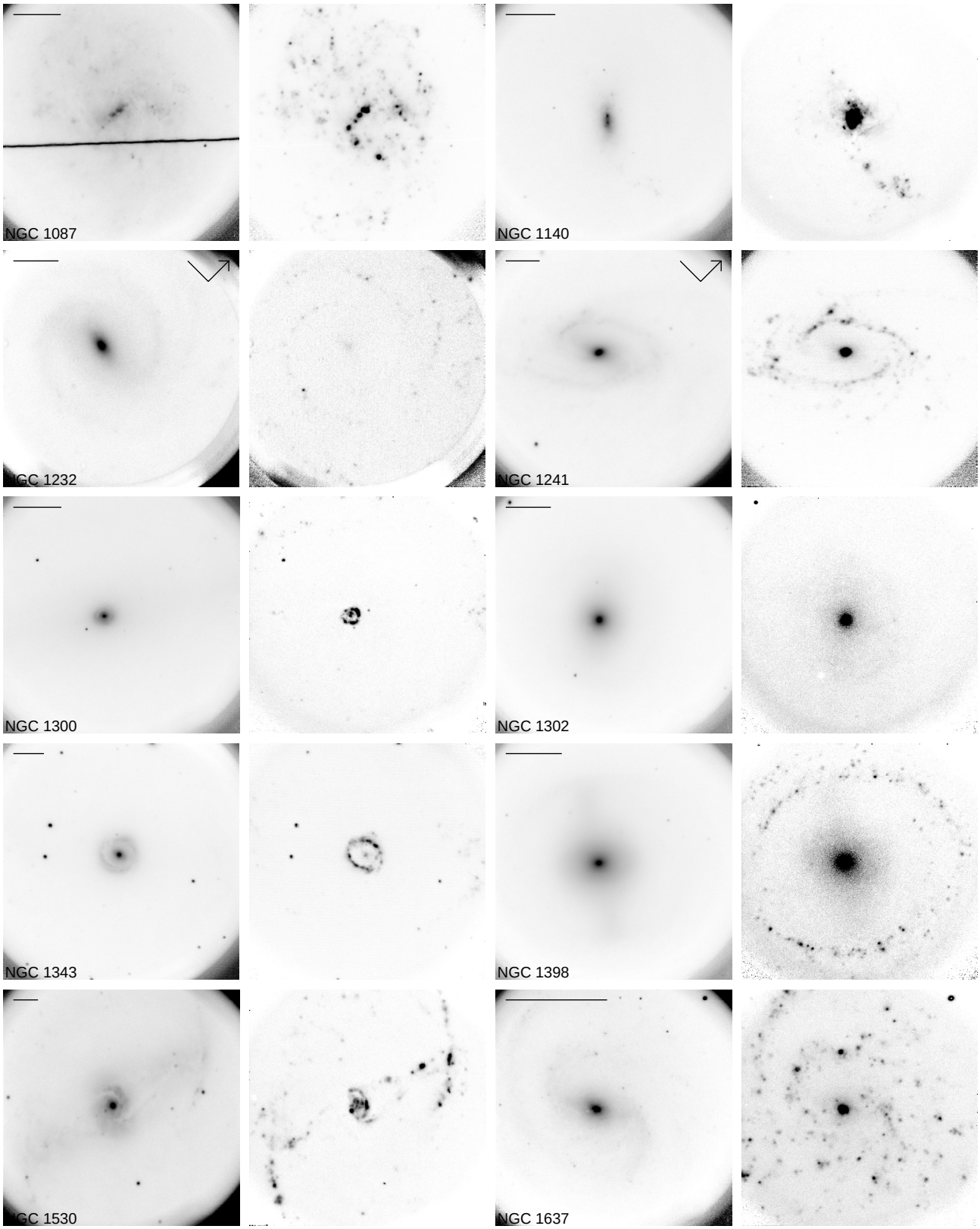

Fig. 1. continued.

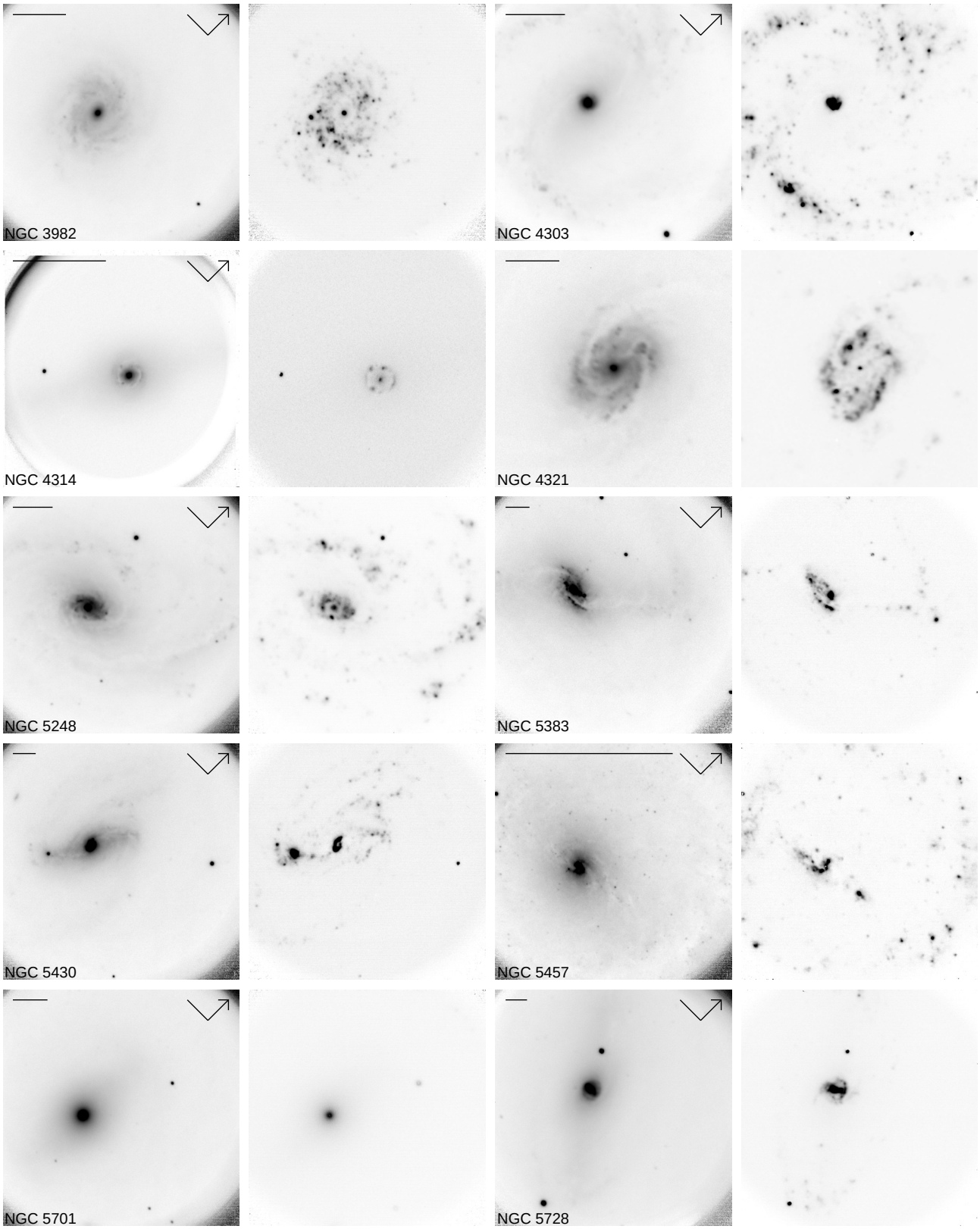

Fig. 1. continued.

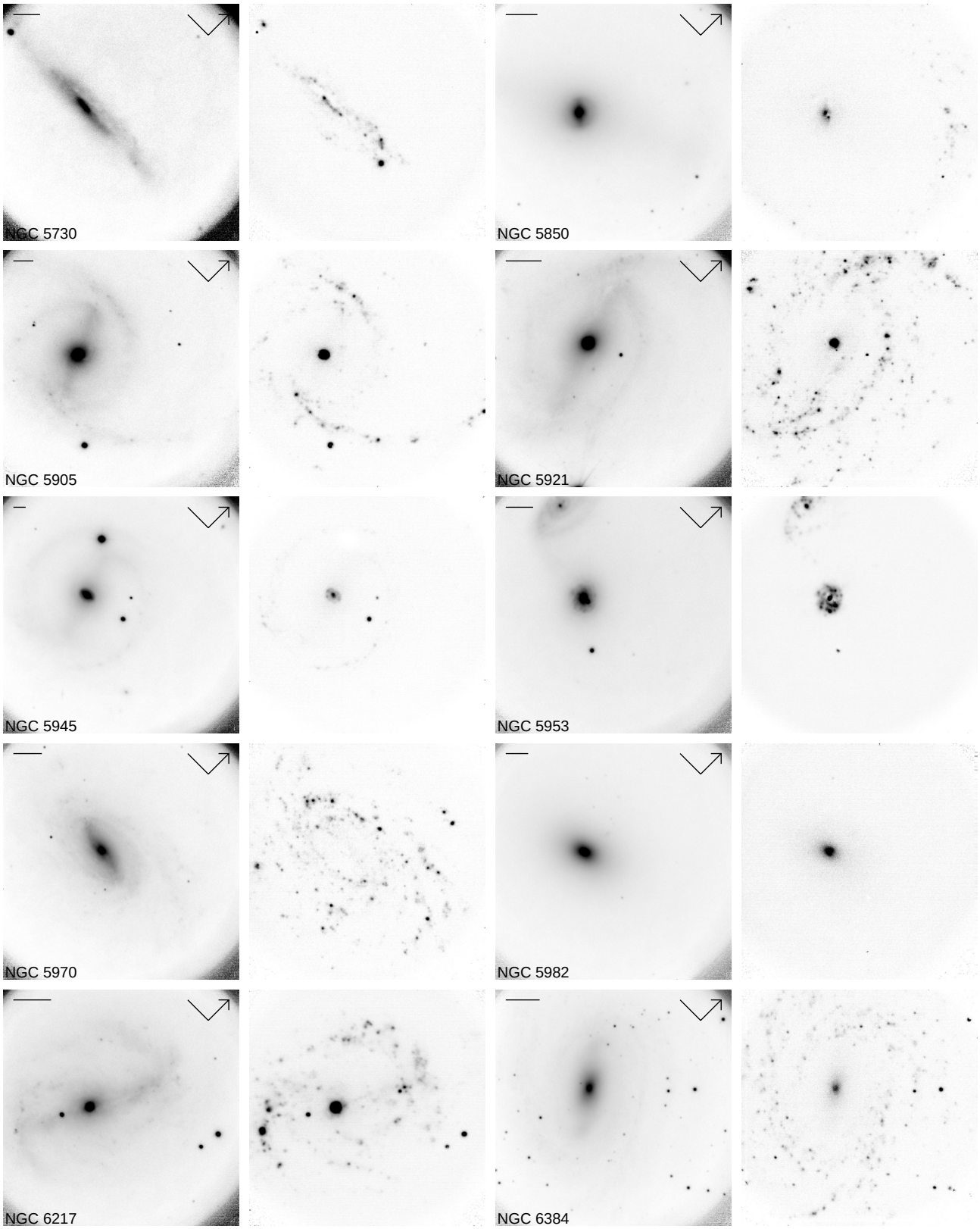

Fig. 1. continued.

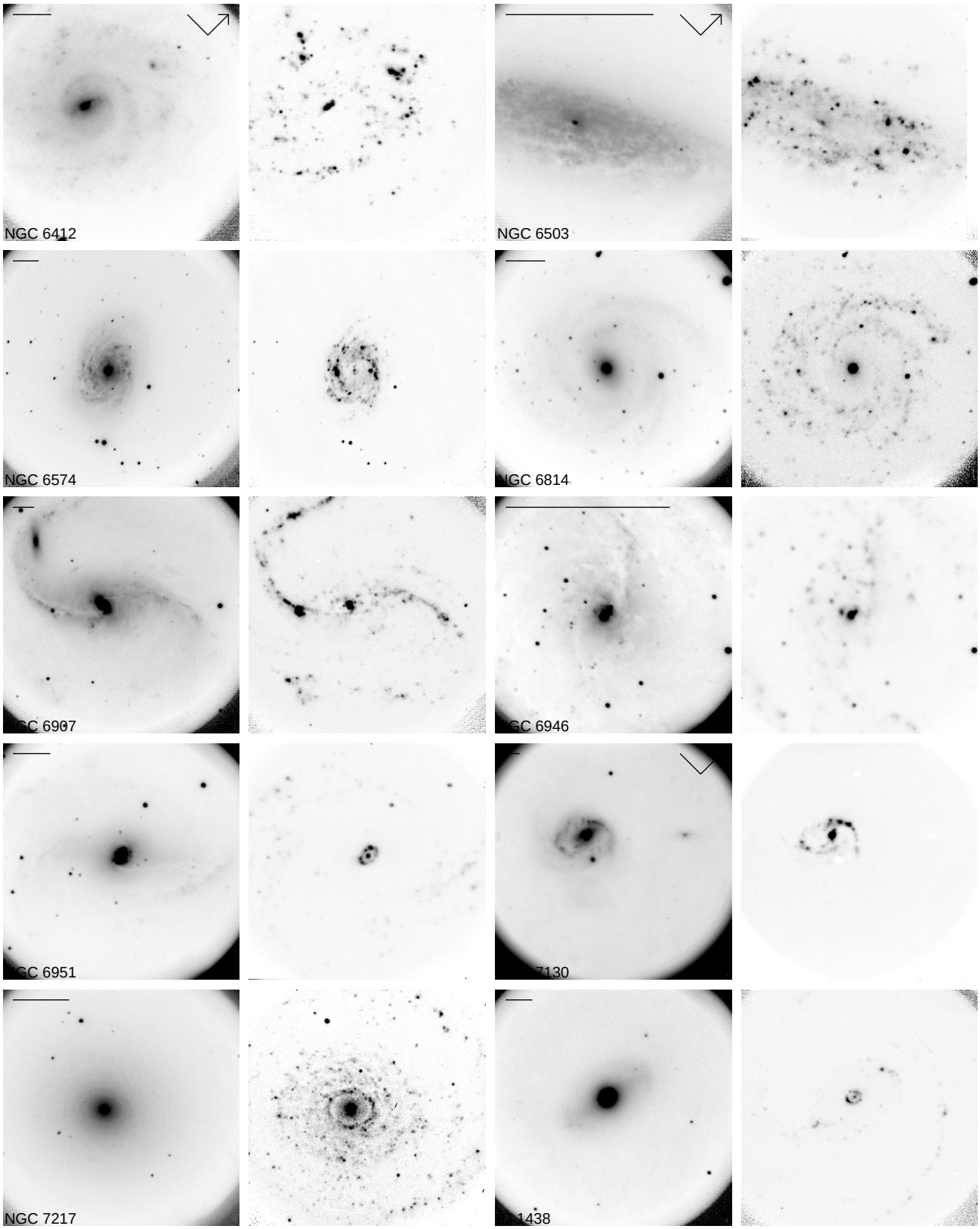

Fig. 1. continued.

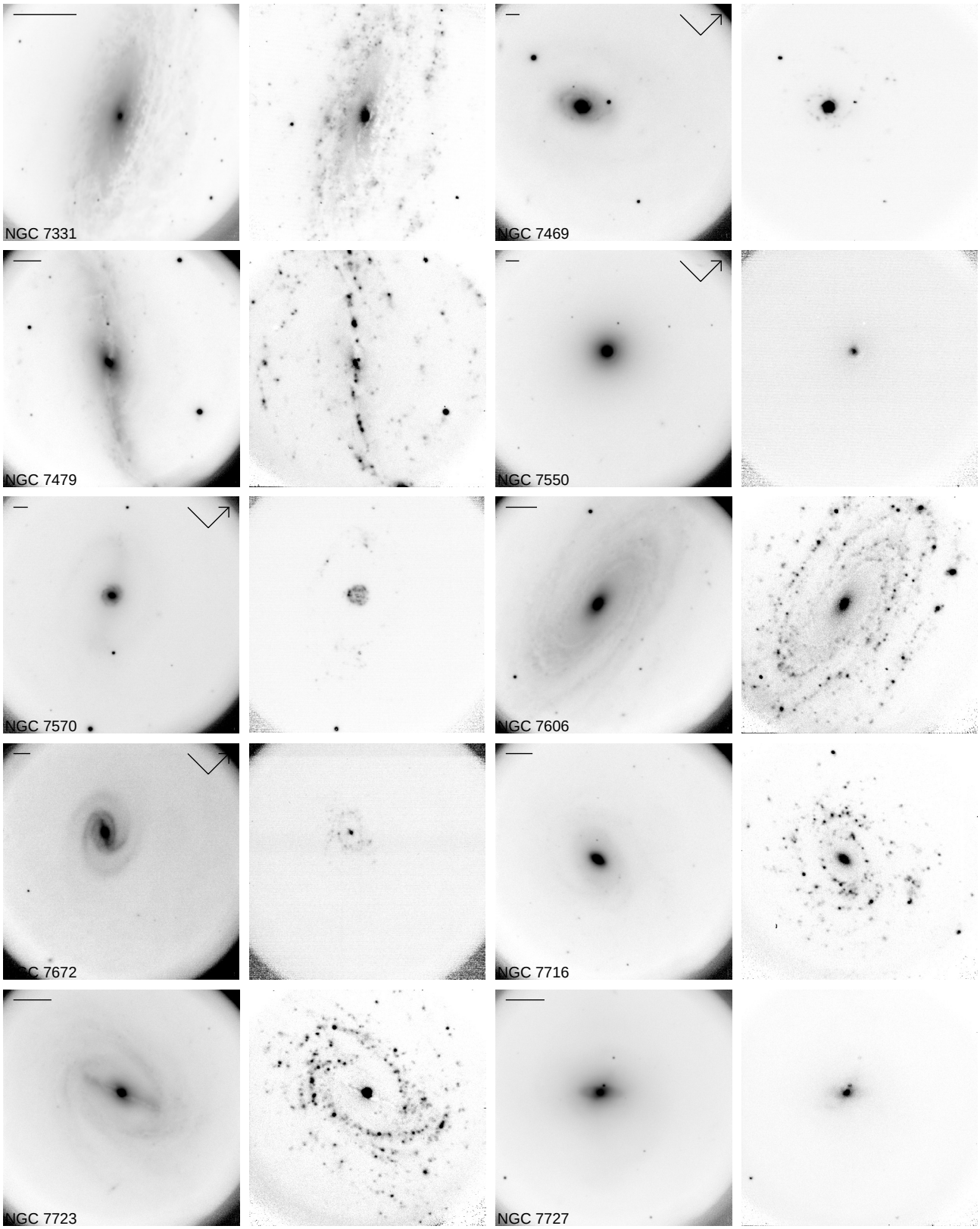

Fig. 1. continued.

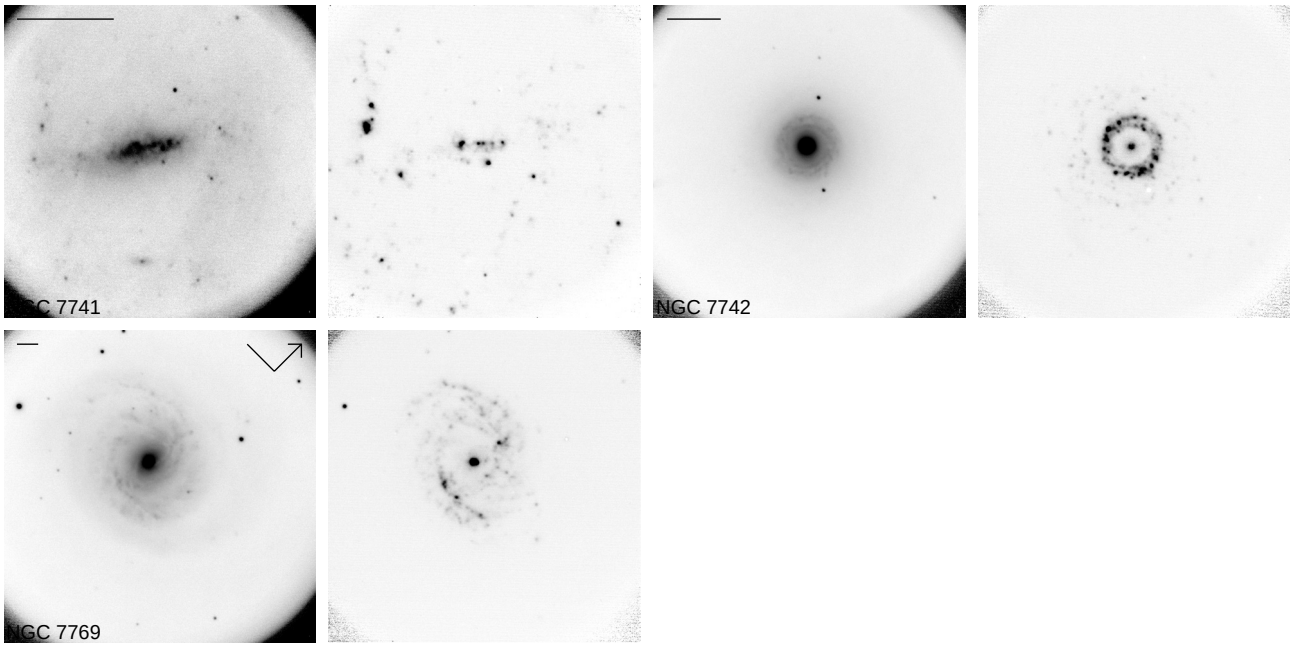

Fig. 1. continued.